

---

# Distributional Sliced-Wasserstein and Applications to Generative Modeling

---

Khai Nguyen<sup>1,2</sup> Nhat Ho<sup>3</sup> Tung Pham<sup>1,4</sup> Hung Bui<sup>1</sup>

## Abstract

Sliced-Wasserstein distance (SWD) and its variation, Max Sliced-Wasserstein distance (Max-SWD), have been widely used in the recent years due to their fast computation and scalability when the probability measures lie in very high dimension. However, these distances still have their weaknesses. In particular, SWD requires several projection samples to approximate its value because it uses the uniform distribution to sample projecting directions while Max-SWD uses only one projection which causes it to lose a large amount of information. In order to account for these weaknesses, we propose a novel distance that finds optimal penalized probability measure over the slices, which is named Distributional Sliced-Wasserstein distance (DSWD). We show that the DSWD is a generalization of both SWD and Max-SWD, and the proposed distance could be found by searching for the push-forward measure over a set of measures satisfying certain constraints. Moreover, similar to SWD, we can extend Generalized Sliced-Wasserstein distance (GSWD) to Distributional Generalized Sliced-Wasserstein distance (DGSWD) by taking advantage of non-linear projection in capturing the structure of the target measures. Finally, we carry out extensive experiments to demonstrate the favorable generative modeling performances of our distances over the previous sliced-based distances in large-scale real datasets.

## 1. Introduction

Optimal Transport (OT) is a classical problem in mathematics and operation research. Due to its appealing theoretical properties and flexibility in practical applications, it has recently become an important tool in data science and machine learning community; see for example, (Courty et al., 2017; Arjovsky et al., 2017; Tolstikhin et al., 2017; Gulrajani et al., 2017) and references therein. However, methods using OT suffer from expensive computational complexity in high dimensional space. That limitation becomes the main obstacle to prevent the use of optimal transport and in particular Wasserstein distance in practical applications.

Recently, several numerical methods have been proposed to speed up the computation of Wasserstein distance. There are two main approaches: entropic regularization-based methods and sliced-based methods. The first approach regularizes the original OT problem with an entropy of the probability measures (Cuturi, 2013; Cuturi & Peyré, 2016). It provides a fast way to approximate Wasserstein distance via the Sinkhorn algorithm (Sinkhorn, 1974; Knight, 2008), which is a non-negative matrix scaling algorithm. The complexities of Sinkhorn algorithm and its variations, such as Greenkhorn and Randkhorn algorithms, were studied carefully in (Altschuler et al., 2017; Lin et al., 2019a;b). Due to the favorable computation of Sinkhorn algorithm, it has been used in many application domains of OT (Courty et al., 2014; Genevay et al., 2017; Patrini et al., 2018; Bunne et al., 2019). However, the Sinkhorn algorithm suffers from the overflowing problem, which breaks its iterative procedure (Chizat et al., 2016; Peyré & Cuturi, 2019). In order to solve that problem, many stabilized versions were proposed (Chizat et al., 2016; Schmitzer, 2019). Nevertheless, these iterative algorithms are still rather unstable and have a high memory requirement, especially in applications which involve deep learning and auto-differentiable framework. On the other hand, the second approach for speeding up the computation of Wasserstein distance is based on a special case of Wasserstein distance. In particular, Wasserstein distance has a closed-form expression for one-dimensional measures, which can be efficiently approximated. It leads to the idea of Sliced-Wasserstein distance (SWD) (Bonneel et al., 2015), which computes the distance between two one-dimension measures obtained by Radon Transform (RT) (Helgason, 2010) and then repeat this procedure uniformly to average

---

<sup>1</sup>VinAI Research <sup>2</sup>Hanoi University of Science and Technology <sup>3</sup>Department of EECS, University of California, Berkeley <sup>4</sup>Faculty of Mathematics, Mechanics and Informatics, Hanoi University of Science, Vietnam National University. Correspondence to: Khai Nguyen <v.khainb@vinai.io>, Nhat Ho <minhnhat@berkeley.edu>, Tung Pham <v.tungph4@vinai.io>, Tung Pham <tungp@vnu.edu.vn>, Hung Bui <v.hungbh1@vinai.io>.

these distances. The SWD not only has solid theoretical properties but also requires much lower computation cost than the high dimensional Wasserstein distance. As a consequence, it provides a scalable way to compute Wasserstein distance and has successfully been applied to a variety of practical tasks (Deshpande et al., 2017; Liutkus et al., 2018; Kolouri et al., 2018; Wu et al., 2019; Deshpande et al., 2019) in which it has been shown to have comparative performances to existing distances and divergences.

Besides those two main approaches, there are also a few different approaches for scaling up the expensive computation of Wasserstein distance in high dimensional settings. In particular, (Paty & Cuturi, 2019) extended the projecting idea of SWD to project probability measures into a lower dimension linear subspace that maximizes their transportation cost. This approach also can reduce the computational cost of Wasserstein distance in high dimension; however, it does not have the advantage of closed-form expression of Wasserstein distance in one dimension space and also needs to have the information of the dimension of that subspace. Another approach is Projected Wasserstein distance (PWD), which was proposed by (Rowland et al., 2019). That distance uses sliced decomposition to find multiple one-dimension optimal transport maps. Then, we compute the average cost of those maps in the original dimension. In the same paper, the authors combined PWD with orthogonal coupling in Monte Carlo estimation to improve the quality of the average step.

Back to the Sliced-Wasserstein distance, the performance of SWD depends on the number of projections and the importance of these projections. In practice, the data often lie in a low dimensional manifold embedded in a high dimensional space. Hence, SWD requires many projections to capture important directions, meanwhile it still has to keep all other unuseful directions, since it does not distinguish between them (Liutkus et al., 2018). In order to account for these issues, (Deshpande et al., 2019) extended SWD to Max Sliced-Wasserstein distance (Max-SWD), which aims to find a single linear projection that maximizes the distance of the probability measures in the projected space. Another way to improve the quality of projections is by using Generalized Radon Transforms (GRT) (Beylkin, 1984). The idea is to replace the linear projecting of Radon Transform on a hyperplane by non-linear projection on an hypersurface. By using GRT, (Kolouri et al., 2019) introduced a novel distance, named Generalized Sliced-Wasserstein distance (GSWD), and also the maximum version, Max Generalized Sliced-Wasserstein distance (Max-GSWD). Although GSWD uses non-linear projections, both GSWD and SWD treat every projection similarly despite the fact that a lot of projections may not be helpful in separating the two target probability measures. The maximum approach (Max-SWD and Max-GSWD) can find the most important projection but it only “observes” target measures via a single projection,

which causes it to ignore useful information about structures of probability measures in high dimension.

**Our contributions.** Our main contributions are four-fold:

- We introduce a novel distance, named Distributional Sliced Wasserstein distance (DSWD) and its empirical version. Our main idea is to search for not just a single most important slice, but a distribution over slices that could balance between expansion of the space spanned by the directions, and the informativeness of directions themselves (i.e., how well they can distinguish the two distributions).
- We propose to search for the best distribution over slices by reparameterizing the space of probability measures over slices as push-forward measures.
- We apply the proposed distances to generative modeling tasks including density estimation and joint contrastive inference. The experiments show that Distributional Sliced-Wasserstein distance performs significantly better than Cramer-Wold distance, Sliced-Wasserstein distance and Max Sliced-Wasserstein distance on these tasks.
- We further extend the Generalized Sliced-Wasserstein distance (GSWD) to Distributional Generalized Sliced-Wasserstein distance and demonstrate that our idea also works well using non-linear projections.

**Organization.** The remainder of the paper is organized as follows. In Section 2, we provide necessary backgrounds for Wasserstein distance and its slice-based versions. In Section 3, we propose Distributional (Generalized) Sliced-Wasserstein distance and analyze some of its theoretical properties. We describe applications of the proposed distances to generative modeling in Section 4 and provide extensive experiment results in Section 5 while concluding the paper with a few discussions in Section 6.

## 2. Background

In this section, we provide necessary backgrounds for the Wasserstein distance, the (Generalized) Radon transform, the (Generalized) Sliced-Wasserstein distance, and the Max (Generalized) Sliced-Wasserstein distance.

### 2.1. Wasserstein Distance

Let  $\mathcal{P}_p(\Omega)$  be the set of Borel probability measures with finite  $p$ -th moment defined on a given metric space  $(\Omega, d)$  and  $\mu, \nu$  in order are probability measures defined on  $X, Y \subseteq \Omega$ , with corresponding probability density functions  $I_\mu$  and  $I_\nu$ . Then, the Wasserstein distance of order  $p \in [1, \infty]$  between

$\mu$  and  $\nu$  is given by (Villani, 2008; Peyré & Cuturi, 2019):

$$W_p(\mu, \nu) = \left( \inf_{\pi \in \Pi(\mu, \nu)} \int_{X \times Y} d^p(x, y) d\pi(x, y) \right)^{\frac{1}{p}},$$

where  $d(\cdot, \cdot)$  is a given cost function,  $\Pi(\mu, \nu)$  is set of all transportation plans  $\pi \in \Pi(\mu, \nu)$  such that their marginal distributions are  $\mu$  and  $\nu$ . In this paper, we abuse notation by using both  $W_p(\mu, \nu)$  and  $W_p(I_\mu, I_\nu)$  for the Wasserstein distance. When  $\mu, \nu$  are absolutely continuous probability measures, the Wasserstein distance between  $\mu$  and  $\nu$  can be equivalently obtained by Monge formulation:

$$W_p(\mu, \nu) = \left( \inf_{f \in MP(\mu, \nu)} \int_X d^p(x, f(x)) d\mu(x) \right)^{\frac{1}{p}}, \quad (1)$$

where  $MP(\mu, \nu) = \{f : X \rightarrow Y | f_{\#}\mu = \nu\}$  is the set of pushforward mappings and  $f_{\#}\mu$  represents for pushforward of measure  $\mu$  through function  $f$ , which is given by:

$$\int_A df_{\#}\mu(y) = \int_{f^{-1}(A)} d\mu(x) \text{ for any Borel set } A \subseteq Y.$$

When  $\mu$  and  $\nu$  are *one-dimension* measures, Wasserstein distance between  $\mu$  and  $\nu$  has a closed-form expression. In particular, let  $F_\mu$  and  $F_\nu$  be the cumulative distribution function (CDF) of  $I_\mu$  and  $I_\nu$ , respectively. The Wasserstein distance between  $\mu$  and  $\nu$  has the following form:

$$W_p(\mu, \nu) = \left( \int_0^1 d^p(F_\mu^{-1}(z), F_\nu^{-1}(z)) dz \right)^{\frac{1}{p}}. \quad (2)$$

## 2.2. Radon Transform and Generalized Radon Transform

The *standard* Radon Transform maps a function  $I \in L^1(\mathbb{R}^d)$  to the space of functions defined over space of lines in  $\mathbb{R}^d$ . In particular, it is defined in (Helgason, 2010) as follows:

$$\mathcal{R}I(t, \theta) = \int_{\mathbb{R}^d} I(x) \delta(t - \langle x, \theta \rangle) dx \quad (3)$$

where  $t \in \mathbb{R}$  and  $\theta \in \mathbb{S}^{d-1} \subset \mathbb{R}^d$  which stands for unit vector on the unit sphere,  $\delta$  is the one-dimensional Dirac delta function and  $\langle \cdot, \cdot \rangle$  is the Euclidean inner-product.

The *generalized* Radon Transform (Beylkin, 1984) extends the original one from integration over hyperplanes of  $\mathbb{R}^d$  to integration over hypersurfaces. The GRT is defined as:

$$\mathcal{G}I(t, \theta) = \int_{\mathbb{R}^d} I(x) \delta(t - g(x, \theta)) dx \quad (4)$$

where  $g$  is a *defining function* and  $\theta \in \Omega_\theta$  (Beylkin, 1984), for example  $g(x, \theta) = \|x - r * \theta\|_2$  with  $r \in \mathbb{R}^+$  and  $\Omega_\theta = \mathbb{S}^{d-1}$ . When  $g$  is the inner product function then GRT becomes RT.

The empirical version of the density ( $I$ ), its Radon transform ( $\mathcal{R}I$ ) and its Generalized Radon Transform ( $\mathcal{G}I$ ) are defined as follows:  $I(x) = \frac{1}{N} \sum_{i=1}^N \delta(x - x_i)$ ,  $\mathcal{R}I(t, \theta) = \frac{1}{N} \sum_{i=1}^N \delta(t - \langle x_i, \theta \rangle)$  and  $\mathcal{G}I(t, \theta) = \frac{1}{N} \sum_{i=1}^N \delta(t - g(x_i, \theta))$ .

## 2.3. Sliced-Wasserstein and Generalized Sliced-Wasserstein Distances

The sliced-Wasserstein distance and Generalized Sliced-Wasserstein distance between two probability measures  $\mu$  and  $\nu$  are formally defined as:

$$SW_p(\mu, \nu) = \left( \int_{\mathbb{S}^{d-1}} W_p^p(\mathcal{R}I_\mu(\cdot, \theta), \mathcal{R}I_\nu(\cdot, \theta)) d\theta \right)^{\frac{1}{p}},$$

$$GSW_p(\mu, \nu) = \left( \int_{\Omega_\theta} W_p^p(\mathcal{G}I_\mu(\cdot, \theta), \mathcal{G}I_\nu(\cdot, \theta)) d\theta \right)^{\frac{1}{p}}.$$

Here, we first get one-dimension marginal measures of two original target measures by Radon Transform or Generalized Radon Transform; then compute a Wasserstein-slice distance by using the close-form Wasserstein distance for one dimension. Then we combine all Wasserstein-slices with *equal* weights. These two are well-defined distances because they are positive-definite, symmetric and satisfy the triangle inequality (Bonnotte, 2013), (Kolouri et al., 2019). The two integrals are usually intractable, however, they can be approximated by using Monte Carlo scheme that draws samples  $\theta_i$  from the uniform distribution on  $\mathbb{S}^{d-1}$  ( $\Omega_\theta$ ):

$$SW_p(\mu, \nu) \approx \left( \frac{1}{N} \sum_{i=1}^N W_p^p(\mathcal{R}I_\mu(\cdot, \theta_i), \mathcal{R}I_\nu(\cdot, \theta_i)) \right)^{\frac{1}{p}},$$

$$GSW_p(\mu, \nu) \approx \left( \frac{1}{N} \sum_{i=1}^N W_p^p(\mathcal{G}I_\mu(\cdot, \theta_i), \mathcal{G}I_\nu(\cdot, \theta_i)) \right)^{\frac{1}{p}}.$$

## 2.4. Max Sliced-Wasserstein and Max Generalized Sliced-Wasserstein Distances

As discussed in the previous section, the uniform random slices could lead to underestimating the discrepancy between two probability measures. In order to address this issue, (Deshpande et al., 2017) propose using neural network to find a discriminating subspace where the projections of both measures are separated. Another effort to overcome the problem is Max Sliced-Wasserstein Distance (Max-SWD) (Deshpande et al., 2019) that defines the distance only on the best slice in discriminating two measures. Combine with “non-linear projecting”, it can lead to Max Generalized Sliced-Wasserstein Distance (Max-GSWD) (Kolouri et al., 2019). Definitions of those distances are as follows:

$$\max SW_p(\mu, \nu) = \max_{\theta \in \mathbb{S}^{d-1}} W_p(\mathcal{R}I_\mu(\cdot, \theta), \mathcal{R}I_\nu(\cdot, \theta)), \quad (5)$$

$$\max GSW_p(\mu, \nu) = \max_{\theta \in \Omega_\theta} W_p(\mathcal{G}I_\mu(\cdot, \theta), \mathcal{G}I_\nu(\cdot, \theta)). \quad (6)$$

## 3. Distributional Sliced-Wasserstein Distance

Motivated by the limitations of previous sliced distances, instead of finding one single optimal slice in Max-SWD,

we propose to search for an optimal regularized probability measure over slices. Intuitively, this setup has the benefit of averaging over a distribution over slices of the SW, yet removes the inefficiency associated with uniformly (and hence uninformatively) sampling of directions. The result is the new Distributional Sliced-Wasserstein distance. We prove that it is a well-defined metric, discuss its connection to the existing distances, and more importantly, propose to reparameterize the optimal slice distribution as a push-forward measure by a neural network so that the optimization problem can be implemented and solved efficiently with existing deep neural network toolkits.

### 3.1. Definition and Metricity

**Definition 1.** Given two probability measures  $\mu$  and  $\nu$  on  $\mathbb{R}^d$  and  $p \geq 1$ , we define the Distributional sliced-Wasserstein distance (DSWD) of order  $p$  between  $\mu$  and  $\nu$  as follows:

$$\begin{aligned} DSW_p(\mu, \nu; C) &= \sup_{\sigma \in \mathbb{M}_C} \left( \mathbb{E}_{\theta \sim \sigma} [W_p^p(\mathcal{R}I_\mu(\cdot, \theta), \mathcal{R}I_\nu(\cdot, \theta))] \right)^{\frac{1}{p}}, \quad (7) \end{aligned}$$

where  $\mathcal{R}$  is Radon transform operator,  $\mathbb{M}_C$  is a set of probability measures  $\sigma$  on  $\mathbb{S}^{d-1}$  such that  $\mathbb{E}_{\theta, \theta' \sim \sigma} |\theta^\top \theta'| \leq C$ .

**Theorem 1.** The  $DSW_p$  is a well-defined metric in the space of Borel probability measures with finite  $p$ -th moment. In particular, it is non-negative, symmetric and satisfies the triangle inequality.

*Proof.* We first show that the Distributional Sliced-Wasserstein distance satisfies triangle inequality for any three probability measures  $\mu_1, \mu_2$ , and  $\mu_3$ . Since the definition of Distributional Sliced-Wasserstein distance, for any  $\epsilon > 0$ , we find that

$$\begin{aligned} &DSW_p(\mu_1, \mu_2; C) \\ &\stackrel{(i)}{\leq} \left( \mathbb{E}_{\theta \sim \sigma_\epsilon^*} [W_p^p(\mathcal{R}I_{\mu_1}(\cdot, \theta), \mathcal{R}I_{\mu_2}(\cdot, \theta))] \right)^{\frac{1}{p}} + \epsilon \\ &\stackrel{(ii)}{\leq} \left( \mathbb{E}_{\theta \sim \sigma_\epsilon^*} [(W_p(\mathcal{R}I_{\mu_1}(\cdot, \theta), \mathcal{R}I_{\mu_3}(\cdot, \theta)) \right. \\ &\quad \left. + W_p(\mathcal{R}I_{\mu_3}(\cdot, \theta), \mathcal{R}I_{\mu_2}(\cdot, \theta)))^p] \right)^{\frac{1}{p}} + \epsilon \\ &\stackrel{(iii)}{\leq} \left( \mathbb{E}_{\theta \sim \sigma_\epsilon^*} [W_p^p(\mathcal{R}I_{\mu_1}(\cdot, \theta), \mathcal{R}I_{\mu_3}(\cdot, \theta))] \right)^{\frac{1}{p}} \\ &\quad + \left( \mathbb{E}_{\theta \sim \sigma_\epsilon^*} [W_p^p(\mathcal{R}I_{\mu_3}(\cdot, \theta), \mathcal{R}I_{\mu_2}(\cdot, \theta))] \right)^{\frac{1}{p}} + \epsilon \\ &\leq \sup_{\sigma \in \mathbb{M}_C} \left( \mathbb{E}_{\theta \sim \sigma} [W_p^p(\mathcal{R}I_{\mu_1}(\cdot, \theta), \mathcal{R}I_{\mu_3}(\cdot, \theta))] \right)^{\frac{1}{p}} \\ &\quad + \sup_{\sigma \in \mathbb{M}_C} \left( \mathbb{E}_{\theta \sim \sigma} [W_p^p(\mathcal{R}I_{\mu_3}(\cdot, \theta), \mathcal{R}I_{\mu_2}(\cdot, \theta))] \right)^{\frac{1}{p}} + \epsilon \\ &= DSW_p(\mu_1, \mu_3; C) + DSW_p(\mu_2, \mu_3; C) + \epsilon, \end{aligned}$$

where the existence of  $\sigma_\epsilon^*$  in (i) is from the definition of supremum; inequality in (ii) is due to the triangle inequality with Wasserstein distance of order  $p$ ; inequality in (iii) follows from the application of the Minkowski inequality. By letting  $\epsilon \rightarrow 0$  in the above inequality, we obtain the conclusion with the triangle inequality of Distributional Sliced-Wasserstein distance.

The non-negativity and symmetry of Distributional Sliced-Wasserstein distance follow directly from the non-negativity and symmetry of Wasserstein distance. For the identity property, it is straight-forward that if  $\mu_1 \equiv \mu_2$  then  $DSW_p(\mu_1, \mu_2) = 0$ . On the other hand, if  $DSW_p(\mu_1, \mu_2) = 0$ , an application of CramérWold theorem leads to  $\mu_1 \equiv \mu_2$ .  $\square$

We now give a few comments about the newly defined distance. Recalling that instead of finding a single best projection direction, the  $DSW_p$  finds the best probability measure of slice directions on the unit sphere  $\mathbb{S}^{d-1}$ . Note that the Max Sliced-Wasserstein distance is equivalent to searching for the best Dirac measure on a single point in  $\mathbb{S}^{d-1}$ . Meanwhile, if we fixed the slice measure to be the uniform measure, we recover the Sliced-Wasserstein Distance method. Hence, both the Max Sliced-Wasserstein and the Sliced-Wasserstein are intimately connected to our distance. Our target is to find a probability measure which is in between the best Dirac measure and the uniform measure to exploit the advantages of the two: a probability measure concentrated in low dimensional space where the two target measures are different the most. However to do this, the regularization constraint  $\mathbb{E}_{\theta, \theta' \sim \sigma} |\theta^\top \theta'| \leq C$  plays a crucial part. Observe that  $|\theta^\top \theta'| \leq 1$  for any  $\theta, \theta' \in \mathbb{S}^{d-1}$ . Hence,  $\mathbb{M}_1$  contains all probability measures on the unit sphere. Optimizing over all probability measure will simply return the best Dirac measure, hence when  $C \geq 1$ ,  $DSW_p(\cdot, \cdot; C)$  is the same as the Max Sliced-Wasserstein distance. Decreasing  $C$  from  $1 \rightarrow 0$  introduces a regularization effect on  $\sigma$  that prefers orthogonality among randomly sampled pair of directions. In addition,  $\mathbb{E}_{\theta, \theta' \sim \sigma^k(\mathbb{S}^k)} |\theta^\top \theta'|$  decreases as a function of  $k$ , where  $\sigma^k$  is the uniform measure on sphere  $\mathbb{S}^k$ . That means when  $C$  is small,  $\mathbb{M}_C$  does not contain uniform probability measures on low dimensional space.

### 3.2. Empirical version of Distributional Sliced-Wasserstein Distance

To search for the “best” probability measure, we assume that  $\sigma$  is a pushforward probability measure which is defined as follow: Let  $f$  be a Borel measurable function from  $\mathbb{S}^{d-1}$  to  $\mathbb{S}^{d-1}$ . For any Borel set  $A \subset \mathbb{S}^{d-1}$ , define  $\sigma(A) = \sigma^{d-1}(f^{-1}(A))$ , where  $\sigma^{d-1}$  is the uniform probability measure on  $\mathbb{S}^{d-1}$ . Then for any Borel measurable

function  $g : \mathbb{S}^{d-1} \rightarrow \mathbb{R}$ ,

$$\int_{\theta \sim \sigma} g(\theta) d\sigma(\theta) = \int_{\theta \sim \sigma^{d-1}} (g \circ f)(\theta) d\sigma^{d-1}(\theta). \quad (8)$$

Hence, Definition 1 could be expressed by

$$\sup_{f \in \mathcal{F}} \left\{ \left( \mathbb{E}_{\theta \sim \sigma^{d-1}(\mathbb{S}^{d-1})} [W_p^p(\mathcal{R}I_\mu(\cdot, f(\theta)), \mathcal{R}I_\nu(\cdot, f(\theta)))] \right)^{\frac{1}{p}} - \lambda \mathbb{E}_{\theta, \theta' \sim \sigma^{d-1}(\mathbb{S}^{d-1})} [ |f(\theta)^\top f(\theta')| ] \right\},$$

where  $\mathcal{F}$  is a class of Borel measurable functions from  $\mathbb{S}^{d-1}$  to  $\mathbb{S}^{d-1}$ . The problem is reduced to find the Borel measurable function  $f$ . An empirical version of the above supremum is below.

**Definition 2.** Given  $p \geq 1$  and two probability measures  $\mu_1$  and  $\mu_2$  on  $\mathbb{R}^d$ . For any  $2 \leq n$  vectors  $\theta_1, \dots, \theta_n$  drawing uniformly from the unit sphere  $\mathbb{S}^{d-1}$ , we define the empirical Distributional Sliced-Wasserstein distance of order  $p$  between  $\mu_1$  and  $\mu_2$  with respect to  $\theta_1, \dots, \theta_n$  as follows:

$$\begin{aligned} & \widehat{DS}_{p,n,\lambda}(\mu_1, \mu_2; \{\theta_i\}_1^n) \\ & := \sup_{f \in \mathcal{F}_\phi} \left\{ \left[ \frac{1}{n} \sum_{i=1}^n W_p^p(\mathcal{R}I_{\mu_1}(\cdot, f(\theta_i)), \mathcal{R}I_{\mu_2}(\cdot, f(\theta_i))) \right]^{\frac{1}{p}} \right. \\ & \quad \left. - \frac{\lambda}{n(n-1)} \sum_{1 \leq i \neq j \leq n} |f(\theta_i)^\top f(\theta_j)| \right\}, \quad (9) \end{aligned}$$

where  $\lambda > 0$  is the regularization parameter and  $\mathcal{F}_\phi$  is a family of differentiable functions  $f_\phi : \mathbb{S}^{d-1} \rightarrow \mathbb{S}^{d-1}$ .

The idea of including the penalty function in the formulation of DSWD is to ensure that the samples  $\theta_1, \dots, \theta_n$  under the optimal mapping  $f$  will not get close to each other especially for large  $\lambda$ . Meanwhile, the supremum guarantees that we try to look for directions where the two target distributions are different the most. In particular, its behaviors are summarized in the following lemma.

**Lemma 1.** The empirical version of Distributional Sliced-Wasserstein Distance has the following properties when  $\lambda$  goes to infinity and zero:

(a) When  $\lambda \rightarrow 0$ , equivalently for  $C = 0$  in Definition 1, the empirical DSWD and the DSWD is the Max Sliced-Wasserstein distances (Deshpande et al., 2019).

(b) When  $\lambda \rightarrow \infty$ ,  $n \leq d$  and  $p = 2$ , the following is true

$$\begin{aligned} \widehat{DS}_{2,n,\infty}^2(\mu_1, \mu_2; \{\theta_i\}_1^n) & := \lim_{\lambda \rightarrow \infty} \widehat{DS}_{2,n,\lambda}^2(\mu_1, \mu_2; \{\theta_i\}_1^n) \\ & \leq \frac{1}{n} W_2^2(\mathcal{R}\mu_1(\cdot, \Psi), \mathcal{R}\mu_2(\cdot, \Psi)), \end{aligned}$$

where  $\Psi$  is the linear space formed by vectors  $\psi_i = f(\theta_i)$  for  $i = 1, 2, \dots, n$ ,  $f$  is the function where (9) attains its

supremum and the Radon transform on  $\Psi$  is defined as follows: For any vector  $v \in \Psi$ ,

$$\mathcal{R}I_\mu(v, \Psi) = \int_x I_\mu(x) \prod_{i=1}^n \delta(\langle x - v, \psi_i \rangle) dx. \quad (10)$$

*Proof.* We start with part (a). When  $\lambda \rightarrow 0$ , it means that there is no penalty or constraint on the  $f(\theta_i)$ . The optimal function  $f$  will map every unit vector to the optimal direction where the marginal measures are different the most under the Wasserstein distance. Hence, the value of DSWD approaches that of Max Sliced-Wasserstein distance.

(b) When  $\lambda \rightarrow \infty$  and  $n \leq d$ , the penalty term of (9) goes to 0 under the optimal mapping  $f$ , which indicates that  $|f(\theta_i)^\top f(\theta_j)|$  will equal 0 for  $1 \leq i \neq j \leq n$ . Formally, we obtain that

$$\begin{aligned} \widehat{DS}_{p,n,\infty}(\mu_1, \mu_2; \{\theta_i\}_1^n) & := \lim_{\lambda \rightarrow \infty} \widehat{DS}_{p,n,\lambda}(\mu_1, \mu_2; \{\theta_i\}_1^n) \\ & = \sup_{\{\psi_i\}_{i=1}^n \in O_d(n)} \left[ \frac{1}{n} \sum_{i=1}^n W_p^p(\mathcal{R}I_{\mu_1}(\cdot, \psi_i), \mathcal{R}I_{\mu_2}(\cdot, \psi_i)) \right]^{\frac{1}{p}}, \end{aligned}$$

where  $O_d(n)$  is the set of  $n$  orthonormal vectors in  $\mathbb{R}^d$ . We first note that if random vector  $X_j \sim \mu_j$ , then  $X_j^\Psi \sim \mathcal{R}I_{\mu_j}(\cdot, \Psi)$ , where  $X_j^\Psi$  is the orthogonal projection of  $X_j$  on  $\Psi$ . Moreover,

$$\begin{aligned} & (\mathcal{R}I_{\mu_j}(\cdot, \Psi))(t, \psi_k) = \\ & \int_{\Psi} \int_{\mathbb{R}^d} I_{\mu_j}(x) \prod_{i=1}^n \delta(\langle x - v, \psi_i \rangle) \delta(\langle v - t\psi_k, \psi_k \rangle) dx dv \\ & = \int_x I_{\mu_j}(x) \delta(\langle x - t\psi_k, \psi_k \rangle) dx = \mathcal{R}I_{\mu_j}(t, \psi_k). \end{aligned}$$

Thus,  $\langle X_j^\Psi, \psi_k \rangle$  has distribution function  $\mathcal{R}I_{\mu_j}(\cdot, \psi_k)$ . Since the orthonormality of  $\psi_i$ ,

$$\mathbb{E} \|X_1^\Psi - X_2^\Psi\|^2 = \sum_{i=1}^n \mathbb{E} \| \langle X_1^\Psi, \psi_i \rangle - \langle X_2^\Psi, \psi_i \rangle \|^2.$$

Taking the minimum over constraints  $X_j^\Psi \sim \mathcal{R}I_{\mu_j}(\cdot, \Psi)$ , the LHS becomes  $W_2^2(\mathcal{R}\mu_1(\cdot, \Psi), \mathcal{R}\mu_2(\cdot, \Psi))$ . Use the inequality  $\sum_i \min_x g_i(x) \leq \min_x \sum_i g_i(x)$  and note that  $W_2^2(\mathcal{R}I_{\mu_1}(\cdot, \psi_i), \mathcal{R}I_{\mu_2}(\cdot, \psi_i))$  is not greater than the  $i$ th term of the RHS, the inequality in part (b) is proved.  $\square$

**Remark.** Inequality of part (b) Lemma 1 justifies the supremum in our objective function (9). The equality could happen in the case of two Gaussian measures those share the same set of eigenvectors of their covariance matrices.

**Approximating by neural network:** Since the optimal mapping  $f$  in the formulation of Distributional Sliced-Wasserstein distance is generally intractable to compute, we constrain the function  $f$  to a class of parametric neural network, namely, we only search for the optimal  $f_\phi$  parameterized by its weight  $\phi$ .

### 3.3. Distributional Generalized Sliced-Wasserstein distance

We also extend GSWD to its “distributional” version - Distributional Generalized Sliced-Wasserstein distance. This distance can use the advantage of non-linear projecting in capturing the structure of the target measures. Note that, heuristic approaches such as using Linear Discriminant Analysis, PCA to find important slices will fail in case of non-linear projection via the Generalized Radon Transform.

**Definition 3.** Given two probability measures  $\mu$  and  $\nu$  on  $\mathbb{R}^d$  and  $p \geq 1$ , we define the distributional Generalized Sliced-Wasserstein distance (DGSWD) of order  $p$  between  $\mu$  and  $\nu$  as follows:

$$\begin{aligned} & DGSW_p(\mu, \nu; C) \\ &= \sup_{\sigma \in \mathbb{M}_C} \left( \mathbb{E}_{\theta \sim \sigma} \left[ W_p^p(\mathcal{G}I_\mu(\cdot, \theta), \mathcal{G}I_\nu(\cdot, \theta)) \right] \right)^{\frac{1}{p}}, \quad (11) \end{aligned}$$

where  $\mathcal{G}$  is Generalized Radon transform operator,  $\mathbb{M}_C$  is a set of probability measures  $\sigma$  on compact set of feasible parameter  $\Omega_\theta$  such that  $\mathbb{E}_{\theta_1, \theta_2 \sim \sigma} \frac{|\theta_1^\top \theta_2|}{\|\theta_1\| \|\theta_2\|} \leq C$ .

We can prove that DGSWD is also a proper distance and it has similar properties like DSWD (see the supplementary materials).

## 4. Applications to Generative Modeling

Our DWS distance can potentially be applied in many settings where there is a benefit of employing an optimal-transport type of distance in a computationally efficient manner. In this section, we discuss two general settings where the DSW distance can be immediately applied. The first is a standard generative modeling task where a generative model is fit to a data distribution by minimizing an appropriate divergence. The second is a joint contrastive inference task where both a generative model and inference model are learned jointly, again by minimizing some divergence in the joint space of observed variable and latent variable. In each setting, we apply the Distributional Sliced-Wasserstein distance to these tasks as well as its generalized version, the Distributional Generalized Sliced-Wasserstein distance.

### 4.1. Distributional Sliced-Wasserstein Generator

We first consider a density estimation setting where a generative model  $p_g = G_\theta(p_z)$ , defined as the transformation of a prior  $p_z$  by a generator  $G_\theta$ , is learned to match a given data distribution  $p_d$  in the sense of minimizing some distance (divergence). For example, Vanilla GAN (Goodfellow et al., 2014) uses adversarial training to minimize Jensen Shannon divergence. Replacing the JS-divergence by f-divergences

and Wasserstein-1 distance, we get two other GAN’s variations: f-GANs (Nowozin et al., 2016) and WGAN (Arjovsky et al., 2017). Using Wasserstein distance has the crucial benefit of a smooth and differentiable objective especially when the support of the data and the generative distributions are not the same. According to (Deshpande et al., 2017), using Sliced-Wasserstein Distance, we can enjoy the benefit of the Wasserstein distance and get better speed in training the model. We propose to replace the SWD by DSWD, hence obtaining the Distributional Sliced Wasserstein Generator by solving

$$\min_{\theta} DSW(p_d, G_\theta(p_z)). \quad (12)$$

### 4.2. Distributional Sliced-Wasserstein Joint Contrastive Inference

Learning both a generator and an inference model (i.e., an encoder) is a central task in latent-variable modeling. A general framework for performing this task is called joint contrastive inference (Dumoulin et al., 2016). Let  $p_\theta(z, x) = p(z)p_\theta(x|z)$  be the generative model,  $q_\phi(z|x)$  be an amortized inference model and define the data-induced aggregated joint inference model as  $\hat{q}_\phi(z, x) = p_d(x)q_\phi(z|x)$ . The joint contrastive inference framework then minimizes some divergence between the two structured joint distributions  $p_\theta(z, x)$  and  $\hat{q}_\phi(z, x)$ . This can be seen as a generalized version of amortized inference. There are some well-known examples of this kind of inference such as the Variational Autoencoder (Kingma & Welling, 2013), Adversarially Learned Inference (Dumoulin et al., 2016), Wasserstein Variational Inference (Ambrogioni et al., 2018), etc. By using our DSW distance, we obtain a new joint contrastive inference method which inherits the benefits of optimal transport family of distances, yet remains scalable and computationally efficient. In particular, we learn both a generator and an inference model by solving

$$\min_{\theta, \phi} DSW(\hat{q}_\phi(x, z), p_\theta(z, x)). \quad (13)$$

## 5. Experiments

In this section, we conduct extensive experiments on two generative modeling tasks outlined in section 4. We compare the performance of our distances with other existing sliced-based distances including the SW, Max-SW, and the Cramer-Wold distance (Tabor et al., 2018). We report the quality of the learned generators using the standard FID score (Heusel et al., 2017) together with qualitative results in the form of randomly generated images from the model. In the joint contrastive inference task, we investigate the convergence behavior, the quality of the recognition model via the reconstruction score, and how close the aggregated posterior and the prior is. Additional results including the generator’s training speed using different distances, the FID

score of joint inference contrastive models, as well as additional qualitative results for reconstruction and generation, are also reported in the supplementary material.

### 5.1. Generator Models

Table 1 provides the FID scores of generators trained using different slice-based distances for MNIST and Fashion MNIST datasets. The results demonstrated that using the distributional variants of the SWD (DSWD and DGSWD) during training leads to generators with significantly better FID scores. In addition, the DSWD generator always gives higher FID than the SWD generator when using the same number of projections. This is also true in the context of non-linear projection in GRT with circular function as the defining function. Qualitative results in Figure 1 also consolidate the previous claims where the best samples are obtained from generators trained with DSWD and DGSWD. In particular, the visual quality of the samples improves noticeably and significantly comparing with Max-SWD and SWD.

When working with very high dimensional distributions, even SWD requires a large number of projections to achieve good performance, leading to heavy computational cost. (Deshpande et al., 2017) proposed a trick of learning a feature function  $h_\phi$  which maps data to new feature space that is more manageable in size. When the feature function is fixed, the generator can be trained to match the distribution of features. When the generator is fixed, the feature function tries to tease apart the data empirical features from the generated feature distribution. When dealing with datasets consisting of higher resolution images, we use the same technique but replace the SWD by our DSWD. Let  $h_\phi$  and  $f_\psi$  be the intermediate layers and the output layer of the Discriminator, respectively. We optimize these two objectives independently:

$$\min_{\theta} \text{DSW}(h_\phi(p_d), h_\phi(G_\theta(p_z))), \quad (14)$$

$$\max_{\psi} \max_{\phi} \mathbb{E}_{x \sim p_d} [\log(f_\psi(h_\phi(x)))] + \mathbb{E}_{z \sim p_z} [\log(1 - f_\psi(h_\phi(G_\theta(z))))]. \quad (15)$$

With the above trick, we train generators using CIFAR10 (64x64) and CelebBA (64x64) datasets (Liu et al., 2015). We show some random generated images from learned models in Figure 2, and FID scores in Table 2. We observe similar trends to the previous results. The distributional distance variants help learning models with better FID scores and also helps the models to generate more realistic images and less dependent on the number of projections.

To gain more understanding about the effectiveness of DSWD in training the generator, we evaluated the learned models by measuring a close approximation to the SWD be-

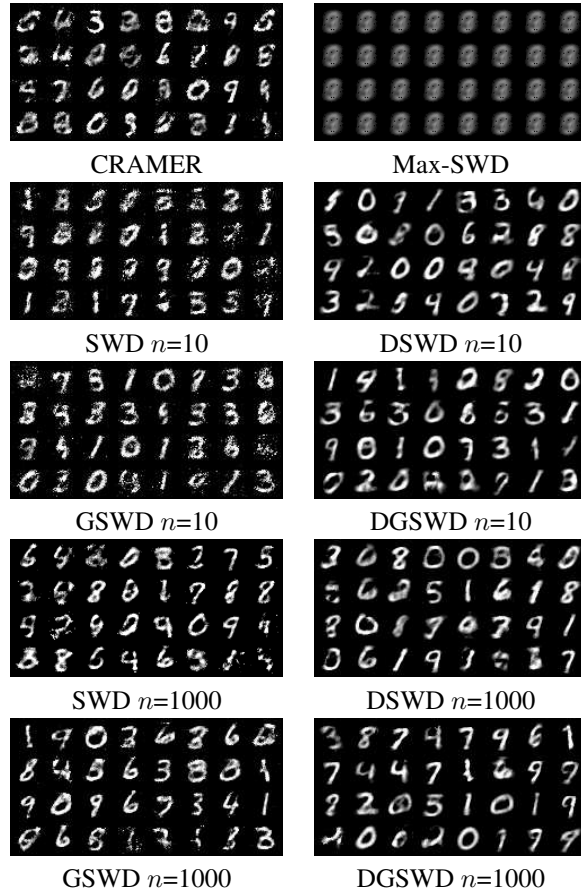


Figure 1. MNIST generated images from generator models based on different distances after 25k training iteration.  $n$  is the number of projections.

Table 1. FID scores of generative models trained using different distances for MNIST and Fashion MNIST.  $n$  is the number of projections used to compute the distances during the training process. Results are averaged from 5 different runs. The hyperparameter  $\lambda$  is tuned by simply trying 4 different values in  $\{1, 10, 100, 1000\}$

| Model                  | n      | MNIST-FID                          | FMNIST-FID                          |
|------------------------|--------|------------------------------------|-------------------------------------|
| Max-SWD                | -      | 404.72 $\pm$ 42.8                  | 483.15 $\pm$ 45.5                   |
| CRAMER                 | -      | 92.77 $\pm$ 1.35                   | 95.11 $\pm$ 0.59                    |
| SWD                    | 10     | 142.2 $\pm$ 4.49                   | 151.34 $\pm$ 2.52                   |
| DSWD( $\lambda=10$ )   | 10     | <b>73.45 <math>\pm</math> 2.97</b> | <b>115.35 <math>\pm</math> 5</b>    |
| SWD                    | $10^3$ | 72.79 $\pm$ 1.45                   | 94.1 $\pm$ 0.48                     |
| DSWD( $\lambda=100$ )  | $10^3$ | <b>57.89 <math>\pm</math> 1.63</b> | <b>83.7 <math>\pm</math> 1.22</b>   |
| GSWD                   | 10     | 130.3 $\pm$ 5.36                   | 160.23 $\pm$ 4.21                   |
| DGSWD( $\lambda=10$ )  | 10     | <b>68.27 <math>\pm</math> 4.57</b> | <b>111.82 <math>\pm</math> 2.43</b> |
| GSWD                   | $10^3$ | 70.39 $\pm$ 1.32                   | 91.36 $\pm$ 0.97                    |
| DGSWD( $\lambda=100$ ) | $10^3$ | <b>56.9 <math>\pm</math> 2.55</b>  | <b>88.32 <math>\pm</math> 1.54</b>  |

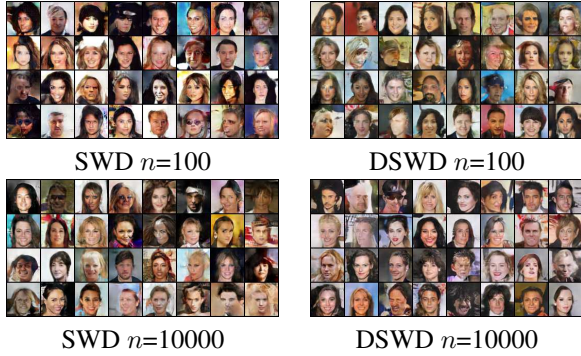


Figure 2. CELEBA generated images from SWD generators and DSWD generators.  $n$  is the number of projections.

Table 2. FID score of generator models trained on CIFAR10 (200 epochs) and CELEBA (100 epochs) dataset (64x64 resolution). Results are averaged from 5 different runs. Max-SWD does not work and hence is excluded.

| Model                   | $n$    | CIFAR10-FID                         | CELEBA-FID                         |
|-------------------------|--------|-------------------------------------|------------------------------------|
| CRAMER                  | -      | 123.23 $\pm$ 4.78                   | 96.2 $\pm$ 1.45                    |
| SWD                     | $10^2$ | 150.64 $\pm$ 7.64                   | 96.43 $\pm$ 2.74                   |
| DSWD ( $\lambda=10$ )   | $10^2$ | <b>115.17 <math>\pm</math> 13.2</b> | <b>90.74 <math>\pm</math> 3.03</b> |
| SWD                     | $10^3$ | 144.75 $\pm$ 4.33                   | 93.17 $\pm$ 2.14                   |
| DSWD ( $\lambda=1000$ ) | $10^3$ | <b>112.81 <math>\pm</math> 4.87</b> | <b>88.25 <math>\pm</math> 3.56</b> |
| SWD                     | $10^4$ | 120.03 $\pm$ 3.38                   | 91.22 $\pm$ 3.35                   |
| DSWD ( $\lambda=1000$ ) | $10^4$ | <b>100.28 <math>\pm</math> 5.67</b> | <b>88.13 <math>\pm</math> 1.27</b> |

tween the learned model distributions and data distribution using a large number of slices and over different training iterations on the MNIST dataset in Figure 3. In order to approximate the SWD, we use 10000 projecting slices drawn uniformly, and 10000 samples each from the two distributions. Figure 3 shows that training using DSWD helps the model distribution converge faster to the data distribution while using the same number of slices. The difference in convergence speed is more pronounced in settings that use a small number of slices, an operating regime that is crucial if computational resources are under constraints.

## 5.2. Joint Contrastive Inference Models

We train joint contrastive models on MNIST using different distances and evaluate how close the two joint latent-observed distributions  $p_\theta(z, x)$  and  $\hat{q}_\phi(z, x)$  are, how close their corresponding marginals are and how well the model reconstructs images. Similar to above, we compute a close approximation of SWD between two distributions using 10000 slices and 10000 samples. The reconstruction loss (L2 distance between original images and reconstructed images) is computed on the MNIST test set. These metrics are measured over many training iterations and shown in Figure

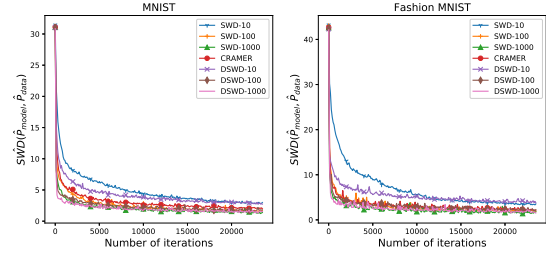


Figure 3. Approximate SWD between the model distribution and the data distribution on MNIST and Fashion MNIST dataset. The number next to SWD and DSWD in the legend is the number of projections used for training the generators.

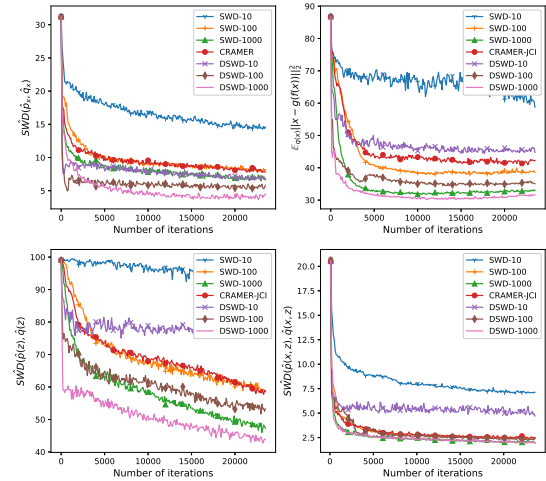


Figure 4. The top-left graph is the changing of approximate SWD between  $p(x)$  and  $q(x)$  over iterations on MNIST dataset. The top-right, bottom-left and bottom-right in order are reconstruction loss on the MNIST test set, approximate SWD between  $p(z)$  and  $q(z)$ , and approximate SWD between  $p(x, z)$  and  $q(x, z)$ .

4. We can see that DSWD achieves better performance than SWD using the same number of slices. Using 100 slices, DSWD dominates the Cramer-Wold distance in every metric. Again, the performance of DSWD is more significantly better than SWD in the important regime where the number of projections more conservative.

## 6. Conclusion

We have presented the Distributional Sliced-Wasserstein distance and Distributional Generalized Sliced-Wasserstein distance, which are novel optimal transport distances between two probability measures. We proved that they are well-defined metrics and provided their theoretical properties. We also compared them to other slice-based distances in a variety of generative modeling tasks, including estimating generative models, and jointly estimating both generators and inference models. Extensive experiments demonstrated



that using the new distances yields better models as well as better convergence behavior during training. Our results showed that these distances have the potential to be used widely in various generative modeling applications.

## References

- Altschuler, J., Weed, J., and Rigollet, P. Near-linear time approximation algorithms for optimal transport via Sinkhorn iteration. In *Advances in neural information processing systems*, pp. 1964–1974, 2017.
- Ambrogioni, L., Güçlü, U., Güçlütürk, Y., Hinne, M., van Gerven, M. A., and Maris, E. Wasserstein variational inference. In *Advances in Neural Information Processing Systems*, pp. 2473–2482, 2018.
- Arjovsky, M., Chintala, S., and Bottou, L. Wasserstein GAN. *arXiv preprint arXiv:1701.07875*, 2017.
- Beylkin, G. The inversion problem and applications of the generalized radon transform. *Communications on pure and applied mathematics*, 37(5):579–599, 1984.
- Bonneel, N., Rabin, J., Peyré, G., and Pfister, H. Sliced and radon Wasserstein barycenters of measures. *Journal of Mathematical Imaging and Vision*, 51(1):22–45, 2015.
- Bonnotte, N. *Unidimensional and evolution methods for optimal transportation*. PhD thesis, Paris 11, 2013.
- Bunne, C., Alvarez-Melis, D., Krause, A., and Jegelka, S. Learning generative models across incomparable spaces. In *International Conference on Machine Learning*, 2019.
- Chizat, L., Peyré, G., Schmitzer, B., and Vialard, F.-X. Scaling algorithms for unbalanced transport problems.(2016). *arXiv preprint arXiv:1607.05816*, 2016.
- Courty, N., Flamary, R., and Tuia, D. Domain adaptation with regularized optimal transport. In *Joint European Conference on Machine Learning and Knowledge Discovery in Databases*, pp. 274–289. Springer, 2014.
- Courty, N., Flamary, R., Tuia, D., and Rakotomamonjy, A. Optimal transport for domain adaptation. *IEEE Transactions on Pattern Analysis and Machine Intelligence*, 39(9):1853–1865, 2017.
- Cuturi, M. Sinkhorn distances: Lightspeed computation of optimal transport. In *Advances in Neural Information Processing Systems*, pp. 2292–2300, 2013.
- Cuturi, M. and Peyré, G. A smoothed dual approach for variational Wasserstein problems. *SIAM Journal on Imaging Sciences*, 9(1):320343, 2016.
- Deshpande, I., Zhang, Z., and Schwing, A. Generative modeling using the sliced Wasserstein distance. In *CVPR*, 2017.
- Deshpande, I., Hu, Y.-T., Sun, R., Pyrros, A., Siddiqui, N., Koyejo, S., Zhao, Z., Forsyth, D., and Schwing, A. Max-sliced Wasserstein distance and its use for GANs. In *CVPR*, 2019.
- Dumoulin, V., Belghazi, I., Poole, B., Mastropietro, O., Lamb, A., Arjovsky, M., and Courville, A. Adversarially learned inference. *arXiv preprint arXiv:1606.00704*, 2016.
- Genevay, A., Peyré, G., and Cuturi, M. Learning generative models with Sinkhorn divergences. *arXiv preprint arXiv:1706.00292*, 2017.
- Goodfellow, I., Pouget-Abadie, J., Mirza, M., Xu, B., Warde-Farley, D., Ozair, S., Courville, A., and Bengio, Y. Generative adversarial nets. In *Advances in neural information processing systems*, pp. 2672–2680, 2014.
- Gulrajani, I., Ahmed, F., Arjovsky, M., Dumoulin, V., and Courville, A. C. Improved training of Wasserstein GANs. In *Advances in neural information processing systems*, pp. 5767–5777, 2017.
- Helgason, S. *Integral geometry and Radon transforms*. Springer Science & Business Media, 2010.
- Heusel, M., Ramsauer, H., Unterthiner, T., Nessler, B., and Hochreiter, S. Gans trained by a two time-scale update rule converge to a local nash equilibrium. In *Advances in Neural Information Processing Systems*, pp. 6626–6637, 2017.
- Kingma, D. P. and Welling, M. Auto-encoding variational Bayes. *arXiv preprint arXiv:1312.6114*, 2013.
- Knight, P. A. The Sinkhorn-Knopp algorithm: convergence and applications. *SIAM Journal on Matrix Analysis and Applications*, 30(1):261–275, 2008.
- Kolouri, S., Pope, P. E., Martin, C. E., and Rohde, G. K. Sliced-Wasserstein autoencoder: an embarrassingly simple generative model. *arXiv preprint arXiv:1804.01947*, 2018.
- Kolouri, S., Nadjahi, K., Simsekli, U., Badeau, R., and Rohde, G. K. Generalized sliced wasserstein distances. *arXiv preprint arXiv:1902.00434*, 2019.
- Lin, T., Ho, N., and Jordan, M. I. On the acceleration of the Sinkhorn and Greenhorn algorithms for optimal transport. *arXiv preprint arXiv:1906.01437*, 2019a.

- Lin, T., Ho, N., and Jordan, M. I. On efficient optimal transport: An analysis of greedy and accelerated mirror descent algorithms. In *International Conference on Machine Learning*, 2019b.
- Liu, Z., Luo, P., Wang, X., and Tang, X. Deep learning face attributes in the wild. In *Proceedings of International Conference on Computer Vision (ICCV)*, December 2015.
- Liutkus, A., Şimşekli, U., Majewski, S., Durmus, A., and Stöter, F.-R. Sliced-wasserstein flows: Nonparametric generative modeling via optimal transport and diffusions. *arXiv preprint arXiv:1806.08141*, 2018.
- Nowozin, S., Cseke, B., and Tomioka, R. f-gan: Training generative neural samplers using variational divergence minimization. In *Advances in neural information processing systems*, pp. 271–279, 2016.
- Patrini, G., Berg, R. v. d., Forré, P., Carioni, M., Bhargava, S., Welling, M., Genewein, T., and Nielsen, F. Sinkhorn autoencoders. *arXiv preprint arXiv:1810.01118*, 2018.
- Paty, F.-P. and Cuturi, M. Subspace robust Wasserstein distances. *arXiv preprint arXiv:1901.08949*, 2019.
- Peyré, G. and Cuturi, M. Computational optimal transport. *Foundations and Trends® in Machine Learning*, 11(5-6): 355–607, 2019.
- Rowland, M., Hron, J., Tang, Y., Choromanski, K., Sarlos, T., and Weller, A. Orthogonal estimation of wasserstein distances. *arXiv preprint arXiv:1903.03784*, 2019.
- Schmitzer, B. Stabilized sparse scaling algorithms for entropy regularized transport problems. *SIAM Journal on Scientific Computing*, 41(3):A1443–A1481, 2019.
- Sinkhorn, R. Diagonal equivalence to matrices with prescribed row and column sums. *Proceedings of the American Mathematical Society*, 45(2):195–198, 1974.
- Tabor, J., Knop, S., Spurek, P., Podolak, I., Mazur, M., and Jastrzebski, S. Cramer-Wold autoencoder. *arXiv preprint arXiv:1805.09235*, 2018.
- Tolstikhin, I., Bousquet, O., Gelly, S., and Schoelkopf, B. Wasserstein auto-encoders. *arXiv preprint arXiv:1711.01558*, 2017.
- Villani, C. *Optimal transport: Old and New*. Springer, 2008.
- Wu, J., Huang, Z., Acharya, D., Li, W., Thoma, J., Paudel, D. P., and Gool, L. V. Sliced Wasserstein generative models. In *Proceedings of the IEEE Conference on Computer Vision and Pattern Recognition*, pp. 3713–3722, 2019.

---

# Supplement to “Distributional Sliced-Wasserstein and Applications to Generative Modeling”

---

## 7. Proof for Distributional Generalized Sliced-Wasserstein distance

Similar proof to the Distributional Sliced-Wasserstein distance:

- Distributional Generalized Sliced-Wasserstein distance satisfies triangle inequality, namely, for any three probability measures  $\mu_1, \mu_2$ , and  $\mu_3$  with the density functions  $I_{\mu_1}, I_{\mu_2}$ , and  $I_{\mu_3}$ , we have

$$\text{DGSW}_p(\mu_1, \mu_2; C) \leq \text{DGSW}_p(\mu_1, \mu_3; C) + \text{DGSW}_p(\mu_3, \mu_2; C).$$

The proof of the above inequality is a direct application of the triangle inequality of Wasserstein distance. In particular, from the definition of Distributional Generalized Sliced-Wasserstein distance, for any  $\epsilon > 0$ , we find that

$$\begin{aligned} \text{DGSW}_p(\mu_1, \mu_2; C) &= \sup_{\sigma \in \mathbb{M}_C} \left( \mathbb{E}_{\theta \sim \sigma} [W_p^p(\mathcal{G}I_{\mu_1}(\cdot, \theta), \mathcal{G}I_{\mu_2}(\cdot, \theta))] \right)^{\frac{1}{p}} \\ &\stackrel{(i)}{\leq} \left( \mathbb{E}_{\theta \sim \sigma_\epsilon^*} [W_p^p(\mathcal{G}I_{\mu_1}(\cdot, \theta), \mathcal{G}I_{\mu_2}(\cdot, \theta))] \right)^{\frac{1}{p}} + \epsilon \\ &\stackrel{(ii)}{\leq} \left( \mathbb{E}_{\theta \sim \sigma_\epsilon^*} [(W_p(\mathcal{G}I_{\mu_1}(\cdot, \theta), \mathcal{G}I_{\mu_3}(\cdot, \theta)) + W_p(\mathcal{G}I_{\mu_3}(\cdot, \theta), \mathcal{G}I_{\mu_2}(\cdot, \theta)))^p] \right)^{\frac{1}{p}} + \epsilon \\ &\stackrel{(iii)}{\leq} \left( \mathbb{E}_{\theta \sim \sigma_\epsilon^*} [W_p^p(\mathcal{G}I_{\mu_1}(\cdot, \theta), \mathcal{G}I_{\mu_3}(\cdot, \theta))] \right)^{\frac{1}{p}} + \left( \mathbb{E}_{\theta \sim \sigma_\epsilon^*} [W_p^p(\mathcal{G}I_{\mu_3}(\cdot, \theta), \mathcal{G}I_{\mu_2}(\cdot, \theta))] \right)^{\frac{1}{p}} + \epsilon \\ &\leq \sup_{\sigma \in \mathbb{M}_C} \left( \mathbb{E}_{\theta \sim \sigma} [W_p^p(\mathcal{G}I_{\mu_1}(\cdot, \theta), \mathcal{G}I_{\mu_3}(\cdot, \theta))] \right) \\ &\quad + \sup_{\sigma \in \mathbb{M}_C} \left( \mathbb{E}_{\theta \sim \sigma} [W_p^p(\mathcal{G}I_{\mu_3}(\cdot, \theta), \mathcal{G}I_{\mu_2}(\cdot, \theta))] \right)^{\frac{1}{p}} + \epsilon \\ &= \text{DGSW}_p(\mu_1, \mu_3; C) + \text{DGSW}_p(\mu_3, \mu_2; C) + \epsilon, \end{aligned}$$

where the existence of  $\sigma_\epsilon^*$  in (i) is from the definition of supremum; inequality in (ii) is due to the triangle inequality with Wasserstein distance of order  $p$ ; inequality in (iii) follows from the application of the Minkowski inequality. By letting  $\epsilon \rightarrow 0$  in the above inequality, we obtain the conclusion with the triangle inequality of Distributional Generalized Sliced-Wasserstein distance.

- The non-negativity and symmetry of Distributional Generalized Sliced-Wasserstein distance follow directly from the non-negativity and symmetry of Wasserstein distance. For the identity property, if  $\mu_1 \equiv \mu_2$  then  $\text{DGSW}_p(\mu_1, \mu_2) = 0$ . On the other hand, if Generalized Radon Transform is injective then if  $\text{DGSW}_p(\mu_1, \mu_2) = 0$ , an application of Cramér-Wold theorem leads to  $\mu_1 \equiv \mu_2$ .

## 8. Experiments setting

- We use a single MLP layer with normalized output as the  $f$  function in DSWD and DGSWD. In all experiments, we use norm 2 as ground metric for the Wasserstein distance. For GSWD and DGSWD, we use  $r = 1000$  for circular function.
- Generator architecture was used for MNIST and Fashion MNIST dataset:  
 $z \in \mathbb{R}^{32} \rightarrow FC_{100} \rightarrow ReLU \rightarrow FC_{200} \rightarrow ReLU \rightarrow FC_{400} \rightarrow ReLU \rightarrow FC_{784} \rightarrow ReLU$
- Generator architecture was used for SVHN dataset:  
 $z \in \mathbb{R}^{100} \rightarrow TransposeConv_{256} \rightarrow BatchNorm \rightarrow ReLU \rightarrow TransposeConv_{128} \rightarrow BatchNorm \rightarrow$

$ReLU \rightarrow TransposeConv_{64} \rightarrow BatchNorm \rightarrow ReLU \rightarrow TransposeConv_1 \rightarrow Tanh$

Discriminator architecture was used for SVHN dataset:

First part:  $x \in \mathbb{R}^{32 \times 32 \times 3} \rightarrow Conv_{32} \rightarrow LeakyReLU_{0.2} \rightarrow Conv_{64} \rightarrow BatchNorm \rightarrow LeakyReLU_{0.2} \rightarrow Conv_{128} \rightarrow BatchNorm \rightarrow Tanh$

Second part:  $Conv_1 \rightarrow Sigmoid$

- Generator architecture was used for CELEBA and CIFAR10 dataset  $z \in \mathbb{R}^{100} \rightarrow TransposeConv_{512} \rightarrow BatchNorm \rightarrow ReLU \rightarrow TransposeConv_{256} \rightarrow BatchNorm \rightarrow ReLU \rightarrow TransposeConv_{128} \rightarrow BatchNorm \rightarrow ReLU \rightarrow TransposeConv_{64} \rightarrow BatchNorm \rightarrow ReLU \rightarrow TransposeConv_1 \rightarrow Tanh$

Discriminator architecture was used for SVHN dataset:

First part:  $x \in \mathbb{R}^{64 \times 64 \times 3} \rightarrow Conv_{64} \rightarrow LeakyReLU_{0.2} \rightarrow Conv_{128} \rightarrow BatchNorm \rightarrow LeakyReLU_{0.2} \rightarrow Conv_{256} \rightarrow BatchNorm \rightarrow LeakyReLU_{0.2} \rightarrow Conv_{512} \rightarrow BatchNorm \rightarrow Tanh$

Second part:  $Conv_1 \rightarrow Sigmoid$

- Joint Contrastive inference encoder architecture on MNIST and Fashion MNIST dataset:  
 $x \in \mathbb{R}^{28 \times 28} \rightarrow FC_{400} \rightarrow LeakyReLU_{0.2} \rightarrow FC_{200} \rightarrow LeakyReLU_{0.2} \rightarrow FC_{100} \rightarrow LeakyReLU_{0.2} \rightarrow FC_{32}$
- Joint Contrastive inference decoder architecture on MNIST and Fashion MNIST dataset:  
 $z \in \mathbb{R}^{32} \rightarrow FC_{100} \rightarrow ReLU \rightarrow FC_{200} \rightarrow ReLU \rightarrow FC_{400} \rightarrow ReLU \rightarrow FC_{784} \rightarrow ReLU$

We trained models on MNIST and Fashion MNIST dataset with batch size = 512, learning rate 0.0005, Adam optimizer (betas=(0.5,0.999)). On CELEBA and CIFAR10 dataset we used batch size = 128, learning rate 0.0005, Adam optimizer (betas=(0.5,0.999)).

Pseudo code for DSWD is in Algorithm 1.

---

**Algorithm 1** Distributional Sliced-Wasserstein Distance
 

---

**Input:**  $\{x_i \sim \mu\}_{i=1}^N, \{y_i \sim \nu\}_{i=1}^N$ , order  $p$ , number of slices  $L$ , function  $f_\phi$ , coefficient  $\lambda$ , learning rate  $\alpha$   
 Sample  $\{\theta_l\}_{l=1}^L \sim \mathcal{U}(\mathbb{S}^{d-1})$   
**while**  $\phi$  has not converged **do**  
    $d = 0$ ;  
   **for**  $l = 1$  to  $L$  **do**  
     Compute  $\hat{x}_i = \langle x_i, f_\phi(\theta_l) \rangle$  and  $\hat{y}_i = \langle y_i, f_\phi(\theta_l) \rangle$  for every  $i$ .  
     Sort  $\hat{x}$  and  $\hat{y}$  in ascending order  
      $d = d + \frac{1}{L} \|\hat{x} - \hat{y}\|_p^p$   
   **end for**  
    $d = d^{\frac{1}{p}}$   
    $loss = d - \frac{\lambda}{L(L-1)} \sum_{i=1}^L \sum_{j \neq i} |f_\phi(\theta_i)^\top f_\phi(\theta_j)|$   
    $\phi = \phi + \alpha \nabla_\phi loss$   
**end while**  
**Output:**  $d$

---

## 9. Additional Generator model results

We show generated images on Fashion MNIST dataset in Figure 5, and on CIFAR10 in Figure 6.

Training time per a minibatch (512) on MNIST dataset:

PCA-10: 0.05 (s); PCA-100: 0.054 (s); PCA-1000: 0.06 (s);

SWD-10: 0.003(s); SWD-100: 0.0037(s); SWD-1000: 0.0079(s);

DSWD-10: 0.02(s); DSWD-100: 0.023(s); DSWD-1000: 0.045(s);

Sinkhorn: 0.1 (s); Cramer: 0.14(s);

For PCA approach, we use top principal components as projecting directions for the empirical SWD. For DSWD, we updated the push-forward function 10 times each generator update. And we run 100 iterations for Sinkhorn-Knopp algorithms to compute Sinkhorn distance.

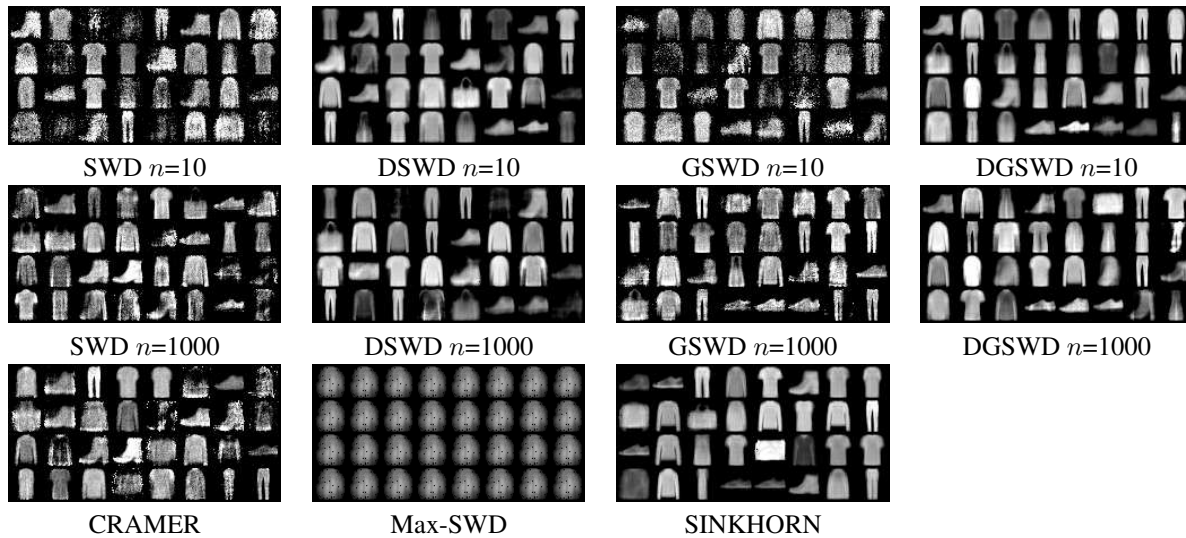


Figure 5. Fashion-MNIST generated images from generator models trained by different distances. For SWD, GSWD, DSWD and DGSWD, "n" means the number of projections.



Figure 6. CIFAR10 generated images from SWD generators and DSWD generators.

## 10. Additional Joint Contrastive Inference results

We show additional results of JCI models included generated images on MNIST and Fashion MNIST in Figure 7, Figure 8; reconstruction loss and FID score in Table 3. Also, we show some reconstructed images from JCI models in Figure 9.

We can see that "distributional" approach improve significantly the results in both images generation and reconstruction.

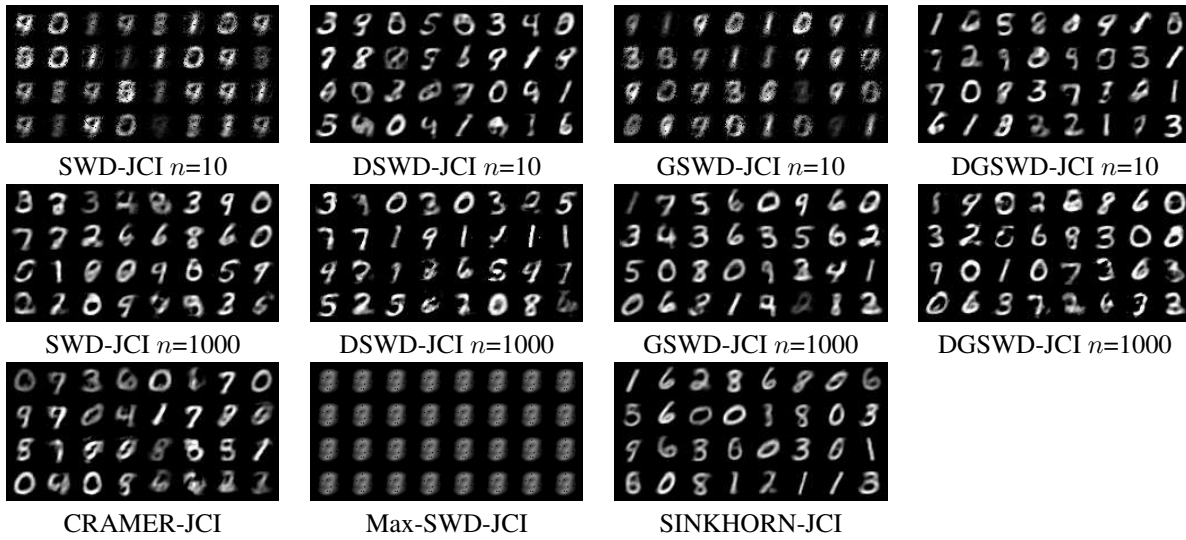


Figure 7. MNIST generated images from joint inference models. For SWD,GSWD, DSWD and DGSWD, "n" means the number of projections.

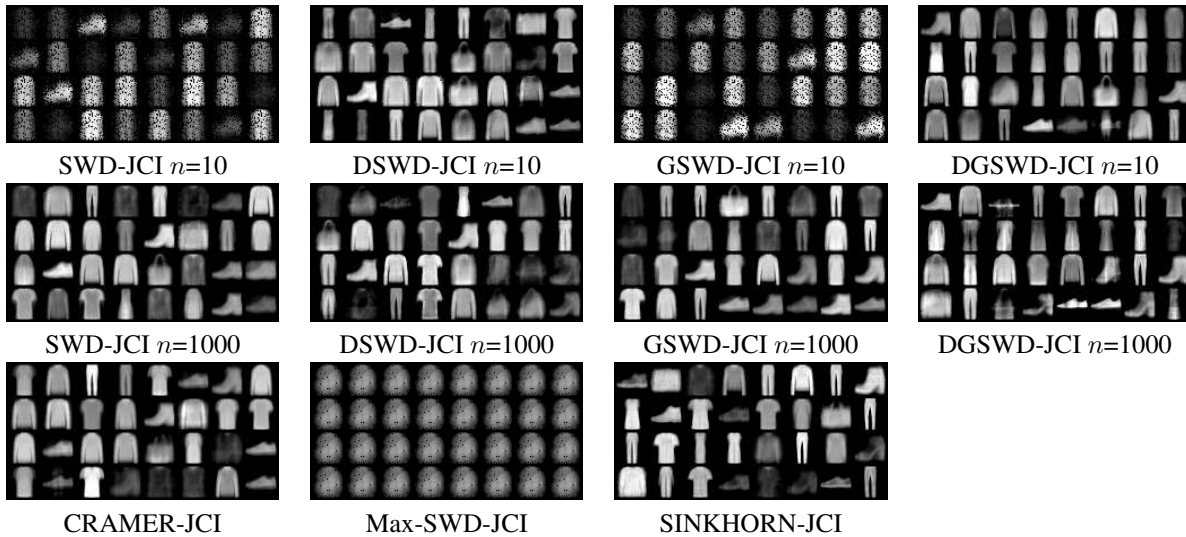


Figure 8. Fashion MNIST generated images from joint inference models. For SWD,GSWD, DSWD and DGSWD, "n" means the number of projections.

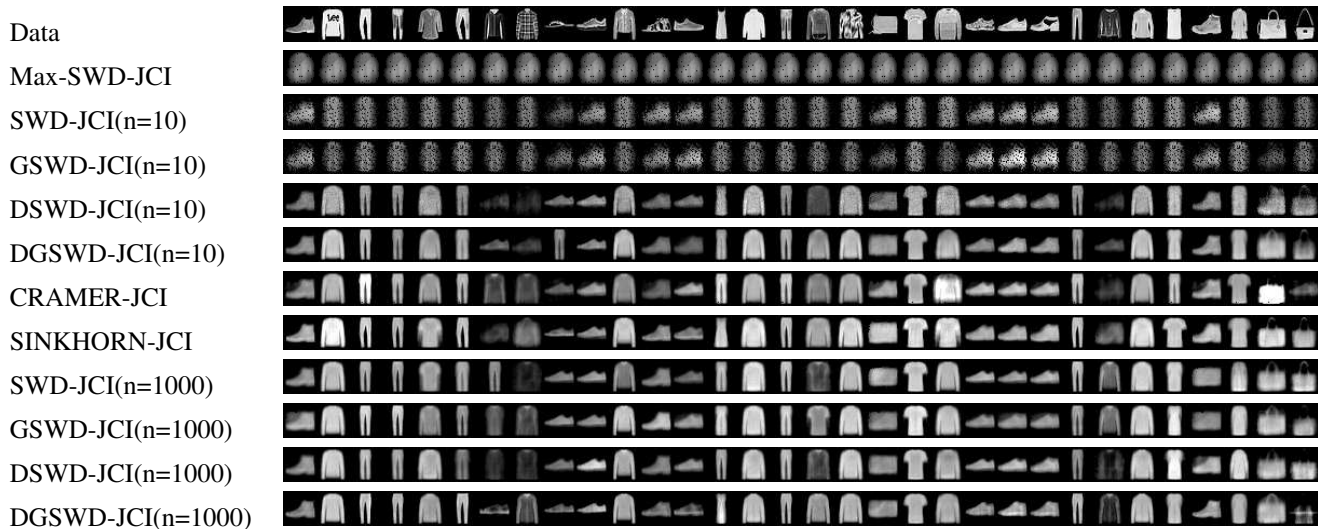


Figure 9. Fashion MNIST dataset reconstructio images ( $n$  is the number of projections). The same phenomenon as MNIST dataset, “distributinal” distances show better performance than other distances.

| Model           | $n$  | MNIST-RCL                          | MNIST-FID                           | FMNIST-RCL                         | FMNIST-FID                          |
|-----------------|------|------------------------------------|-------------------------------------|------------------------------------|-------------------------------------|
| CRAMER-JCI      |      | $42.66 \pm 1.32$                   | $121.9 \pm 2.02$                    | $40.05 \pm 0.52$                   | $157.11 \pm 4.23$                   |
| SINKHORN-JCI    |      | $29.28 \pm 0.93$                   | $80.12 \pm 3.21$                    | $32.46 \pm 0.42$                   | $91.68 \pm 3.45$                    |
| Max-SWD-JCI     |      | $54.28 \pm 0.25$                   | $442.74 \pm 46.22$                  | $71.97 \pm 0.92$                   | $445.82 \pm 36.94$                  |
| SWD-JCI         | 10   | $60.47 \pm 3.27$                   | $252.77 \pm 18.3$                   | $71.460 \pm 2.49$                  | $315.43 \pm 5.62$                   |
| DSWD-JCI(10)    | 10   | <b><math>37.5 \pm 0.49</math></b>  | <b><math>104.59 \pm 3.76</math></b> | <b><math>33.46 \pm 1.47</math></b> | <b><math>127.35 \pm 2.79</math></b> |
| SWD-JCI         | 100  | $38.44 \pm 1.25$                   | $127.18 \pm 5.14$                   | $43.05 \pm 2$                      | $179.48 \pm 3.07$                   |
| DSWD-JCI (100)  | 100  | <b><math>35.54 \pm 0.93</math></b> | <b><math>105.35 \pm 2.11</math></b> | <b><math>37.41 \pm 1.63</math></b> | <b><math>111.8 \pm 2.61</math></b>  |
| SWD-JCI         | 1000 | $33.44 \pm 0.86$                   | $88.51 \pm 3.88$                    | $35.06 \pm 0.7$                    | $124.23 \pm 2.23$                   |
| DSWD-JCI(100)   | 1000 | <b><math>32.27 \pm 0.35</math></b> | <b><math>85.1 \pm 2.63</math></b>   | <b><math>30.75 \pm 1.3</math></b>  | <b><math>90.87 \pm 3.08</math></b>  |
| GSWD-JCI        | 10   | $57.81 \pm 2.31$                   | $233.05 \pm 19.6$                   | $83 \pm 3.58$                      | $305.64 \pm 6.31$                   |
| DGSWD-JCI(10)   | 10   | <b><math>34.48 \pm 0.75</math></b> | <b><math>85.6 \pm 2.86</math></b>   | <b><math>29.9 \pm 1.38</math></b>  | <b><math>115.83 \pm 1.99</math></b> |
| GSWD-JCI        | 100  | $37.42 \pm 1.36$                   | $123.6 \pm 4.74$                    | $42.38 \pm 2.11$                   | $186.69 \pm 4.13$                   |
| DGSWD-JCI (100) | 100  | <b><math>32.85 \pm 0.87</math></b> | <b><math>68.39 \pm 1.87</math></b>  | <b><math>26.54 \pm 2.43</math></b> | <b><math>99.71 \pm 1.52</math></b>  |
| GSWD-JCI        | 1000 | $33.67 \pm 1.16$                   | $86.89 \pm 2.49$                    | $34.35 \pm 0.62$                   | $138.1 \pm 1.03$                    |
| DGSWD-JCI(100)  | 1000 | <b><math>30.53 \pm 0.43</math></b> | <b><math>64.85 \pm 3.33</math></b>  | <b><math>25.6 \pm 0.78</math></b>  | <b><math>91.1 \pm 2.18</math></b>   |

Table 3. Joint Constrastive Inference models RCL and FID